Journal of Power Sources 676 (2026) 239846

Contents lists available at ScienceDirect

Journal of Power Sources

journal homepage: www.elsevier.com/locate/jpowsour

Stainless steel based anode porous transport layers for PEM water electrolysis

Sarah Zerressen [a,*], Tim Sievert [b], Andreas Glüsen [a], Martin Müller [a], Robert Vaßen [b], Ralf Peters [a,c,d], Ulf-Peter Apfel [e,f]

[a] Forschungszentrum Jülich GmbH, Institute of Energy Technologies, IET-4: Electrochemical Process Engineering, 52425, Jülich, Germany
[b] Forschungszentrum Jülich GmbH, Institute of Energy Materials and Devices, IMD-2: Materials Synthesis and Processing, 52425, Jülich, Germany
[c] Ruhr-Universität Bochum, Institute of Thermo- and Fluiddynamics, Synthetic Fuels, 44801, Bochum, Germany
[d] JARA-ENERGY, 52056, Aachen, Germany
[e] Ruhr-Universität Bochum, Activation of Small Molecules/Technical Electrochemistry, 44801, Bochum, Germany
[f] Fraunhofer UMSICHT, Department of Electrosynthesis, 46047, Oberhausen, Germany

HIGHLIGHTS

- 316L-based PTLs with performance close to full titanium PTLs.
- 2.8 A cm^{-2} at 2 V with 316L expanded metal PTL with Ti cold gas spray coated coating.
- 60±12 µm protective Ti-coating enabled stable PEMWE operation for 1006 h.
- 58% Titanium saved compared to full titanium PTLs.

GRAPHICAL ABSTRACT

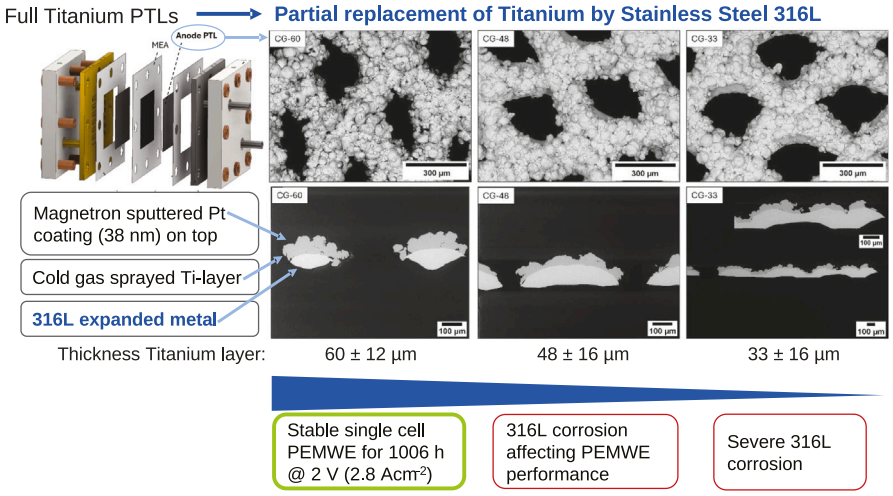

ARTICLE INFO

Keywords:
Water electrolysis
Porous transport layer
Stainless steel
Corrosion protection
Cold gas spraying

ABSTRACT

The energy system and the chemical industry of the present and future require large quantities of hydrogen. A key technology for the production of green hydrogen is the polymer electrolyte membrane water electrolysis (PEMWE). However, investment costs are high due to the use of iridium, platinum and titanium. One way to reduce costs is to partially replace titanium used for the porous transport layers (PTL) by stainless steel. Therefore, we used 316L expanded metals and coated them with titanium by cold gas spraying (CGS) for corrosion protection. Thereby, the average layer thickness was reduced from 60±12 µm to 48±16 µm to 33±16 µm. The corrosion stability of the expanded metals was evaluated by long-term measurements for up to 1006 h at 2.0 V, impedance spectroscopy, analyzing water samples and performing post mortem analysis of cross-sections of the membrane electrode assemblies (MEAs). With 48 µm and 33 µm thick coatings, cationic contamination caused by corrosion lead to increasing ohmic resistances and catalyst inactivation. In contrast, with thicker protective coatings of 60 µm, PEMWE operation was conducted for 1006 h at 2.8 A cm^{-2} without

* Corresponding author.
E-mail address: s.zerressen@fz-juelich.de (S. Zerressen).

https://doi.org/10.1016/j.jpowsour.2026.239846
Received 7 January 2026; Received in revised form 21 February 2026; Accepted 8 March 2026
Available online 11 March 2026

any evidence of corrosion impact and with performance close to state-of-the-art PTLs. With this newly developed PTL, around 58% Ti-savings can be achieved compared to full titanium PTLs.

1. Introduction

Hydrogen is an essential component of basic chemicals like methanol and ammonia, as well as an energy source for steel production [1] and a sustainable way to store electricity from renewable energy sources. At present, hydrogen is largely obtained from fossil sources, which is associated with the emission of CO_2 [2]. To decarbonize the chemical industry and our energy systems, it is of importance to reduce the emission of greenhouse gases caused by the production of hydrogen. Reducing the climate impact of hydrogen production can be achieved by water electrolysis (green hydrogen), with the electricity required provided by renewable energy sources [3]. However, the production of green hydrogen is more expensive than by steam reforming (grey hydrogen). The price of green hydrogen depends on the one hand on the price of electricity and on the other hand on the investment costs of the electrolyzer and system [4]. Iridium, platinum and titanium are used particularly in polymer electrolyte water electrolysis (PEMWE). Current research is therefore focusing on the reduction of the amount of precious metals and titanium required.

One way of replacing titanium is to use stainless steel. A lower price is often argued to be an advantage of stainless steel 316L over titanium [5–8]. However, for a holistic comparison of the materials, their availability, origin and processability, including machine wear and the price for protective coatings must be considered. As such a holistic study of all these aspects would go beyond the scope of this work, it is pointed out that an assessment of the usability of 316L as a base material for anode PTLs can be given. After some studies have dealt with the replacement of titanium by coated stainless steel for the bipolar plates (BPP) in PEMWE [5–7,9], more studies on stainless steel-based PTLs are published [10–13]. Using uncoated stainless steel as anode PTL is not possible due to its instability in contact with the acidic Nafion™ membrane of the catalyst layer (CL) in combination with the anodic polarization up to 1.6 V vs. standard hydrogen electrode (SHE) [14–16]. Corrosion of stainless steel PTLs in PEMWE was demonstrated by Mo et al. [10]. First reports of a 316L composite PTL by Daudt et al. [11] consisting of stainless steel expanded metals with tape casted and screen printed niobium coatings were only competitive with titanium PTLs up to 1 A cm^{-2}. In a subsequent study Bram and Glüsen [17] developed further multi-layer PTLs consisting of stainless steel expanded metals welded with 300 µm thick titanium sintered bodies and attested stable performance over 1500 h, although tarnishing was visible after the experiment on the side of the PTLs facing the flowfield (FF). Stiber et al. [12] developed 316L based BPPs and PTLs coated with titanium and niobium by vacuum plasma spraying (VPS). This layered PTL was corrosion resistant as no iron was found in the membrane-electrode-assembly (MEA) after an 1500 h accelerated stress test (AST). However the aging rate amounted for approximately 270 µV h^{-1}. All losses were attributed to degradation of the MEA. The thickness of the titanium and niobium coatings was not specified, but can be estimated to 45±25 µm and 14±10 µm respectively from scanning electron microscope (SEM) images. Their work marked an important step in the direction of cost-effective anode PTLs, but with VPS, vacuum is still required for the coating process. Therefore, we used cold gas spraying (CGS) as in a previous study to deposit titanium layers for corrosion protection of 316L expanded metal PTLs [13]. Although CGS is not performed under vacuum, the bulk material does not oxidize due to the comparatively low temperature among thermal spray processes of 900 °C during deposition.

However, it has not yet been clarified how thin the thickness of the corrosion protection layer can be reduced to keep the amount of titanium used as minimal as possible while ensuring corrosion protection. Furthermore, it was still unknown whether all metal cations emitted from the stainless steel base have an influence on the half-cell reactions or proton transport or whether occasionally emitted metal cations that are carried out of the cell instead of reaching the anode catalyst layer have no influence on the cell performance. Hence, we systematically reduced the coating thickness and conducted stability experiments with PEMWE single cells for up to 1006 h at a maximum cell voltage of 2.0 V. To evaluate the stability of the 316L expanded metals, water samples were taken from the anode and cathode outlet during the experiments and analyzed via ICP-MS and the PTLs and MEAs were analyzed post mortem by SEM and EDX. The influence of potentially emitted metal cations on the cell performance was investigated by recording I–V curves and impedance spectra.

2. Materials and methods

2.1. Electrolysis cells and test bench

PEMWE single cells and the test bench where five cells can be run simultaneously were described by Rakousky [18] and previous studies [19,20]. Each cell is connected to a power supply, temperature and voltage senses, heating rods and water supply via a peristaltic pump for the anode and cathode side where one pump delivers water separately for the anode and cathode circuit. The water flow rates were 25.0±1.5 mL min^{-1} on the anode and 24.0±2.5 mL min^{-1} on the cathode sides. The incoming water was heated to 80±1 °C using glass heat exchangers and its conductivity was 0.055 µS cm^{-2} and its total organic carbon (TOC) content was below 3 ppb. Excess water that was not consumed by electrolysis was returned to the storage tanks, where it was mixed with fresh water. Ion exchangers (Amberlite® IRN-150) were installed in front of the cell inlet to prevent impurities from entering. The temperature of the end plates was measured by two NiCr-Ni thermocouples and controlled at 80±1 °C using an in-house built temperature control system. A TDK Lambda GEN-20-76 DC power supply was used, and cell voltages were recorded with a sample rate of 10 s by a Keithley model 2701 multimeter.

A drawing of the test cells is given in Figure S1. The flowfield (FF)-plates are manufactured of titanium, are coated with platinum at the anode and gold at the cathode side and include a serpentine flowfield to transport water over the active cell area of 17.64 cm^2. Catalyst coated membranes (CCMs) were manufactured in-house with Nafion™ 117 membranes as described previously [19,20]. The resulting loadings were 0.99±0.07 $mg_{Ir}cm^{-2}$ for the anode catalyst layers and 0.26±0.05 $mg_{Pt}cm^{-2}$ for the cathode catalyst layers.

Commercially available titanium felts (Bekipor® 2GDL10-0.35 from NV Bekaert SA, Belgium) served as standard (benchmark) PTLs on the anode side. The benchmark PTLs were 363±8 µm thick, had 68% porosity and a fiber diameter of 20 µm. Coated 316L expanded metal anode PTLs investigated in this study are described in more detail below. The PTLs were sealed with polytetrafluoroethylene (PTFE) gaskets fitting the PTLs thickness with an accuracy of 5 µm. Carbon paper with a thickness of 367±1 µm (TGP-H-120 from Toray, Japan) was utilized as cathode PTL and compressed by 29% by sealing with a thinner PTFE-gasket (260 µm).

2.2. 316L expanded metals

316L expanded metals with a thickness of 138 µm and an opening of 366±8 µm × 218±5 µm were provided by Bender GmbH Maschinenbau & Streckmetallfabrik (Siegen, Germany). The size of the openings was determined from scanning electron microscopy (SEM) and optical microscope images using the software ImageJ. The composition of the expanded metals was determined via Inductively coupled plasma optical emission spectroscopy (ICP-OES). The resulting fractions are given in Figure S4. Prior to the coating process, all PTLs were cleaned with a laboratory dishwasher (Miele Professional PG 8583) at 90 °C.

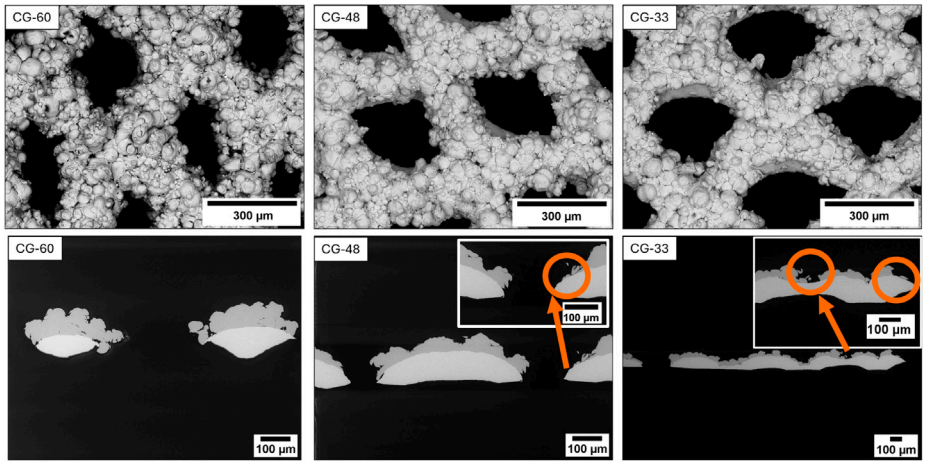

Fig. 1. SEM top view and cross section images of 316L expanded metals with CGS titanium coatings adapted from [25].

Table 1
Coating thickness of titanium CGS coatings on PTLs determined from SEM cross sections and subtraction of the coated PTL thickness and expanded metal as well as the layer weight.

Sample	Coating thickness[1]/µm	Thickness expanded metal with coating[2]/µm	Thickness expanded metal with coating subtracted by thickness expanded metal/µm	Layer weight [25]/gcm^{-2}
CG-33	33 ± 14	196 ± 5	67 ± 6	0.0084
CG-48_1	48 ± 15	226 ± 7	97 ± 7	0.0164
CG-48_2	48 ± 15	242 ± 17	113 ± 10	0.0164
CG-60_1	60 ± 12	300 ± 39	171 ± 20	0.0216
CG-60_2	60 ± 12	319 ± 51	190 ± 26	0.0216

1: Determined from SEM cross sections using the software imageJ; 2: Measured using a thickness gauge.

2.3. Cold gas spraying (CGS)

The deposition of titanium coatings on the CL-facing side of the PTLs by cold gas spraying was conducted at the institute of Materials Synthesis and Processing (IMD-2). The powder used consisted of titanium grade 1 with spherical particles and a particle size distribution of 20 µm to 53 µm and an average particle size of 35±13 µm (TLS Technik GmbH & Co. Spezialpulver KG, Germany). The deposition was conducted with an Impact Innovations GmbH cold spray system and nitrogen as propellant and feedstock carrier gas at a gas inlet temperature of 900 °C.

To control the layer thickness, the powder feed rate was changed from 19.1 g min^{-1} to 28.3 g min^{-1} to 38.3 g min^{-1}. Further details about the coating process are given in our previous study [13]. Within this study we demonstrated that titanium layers were deposited without any oxide phase in the bulk by XRD and EDX mapping. In addition, CGS is known for ensuring the deposition of oxide-free titanium layers [21,22]. Only the native oxide layer, which forms on the surface of the coating after spraying through contact with the atmosphere, cannot be imaged by EDX or XRD due to the limited axial resolution of the methods. However, as the titanium coating is sputtered with platinum, the thin native oxide layer, which is only a few nanometers thick [23], has only a minor effect on the cell performance [24]. As the focus of the work was on analyzing the stability of the stainless steel base, a reduction step for the titanium coating was not performed. The thicknesses of the coatings were determined using SEM images of cross-sections of the coated samples and amounted for 33±16 µm (CG-33), 48±16 µm (CG-48) and 60±12 µm (CG-60). Top view SEM images and cross sections of the coated expanded metals are shown in Fig. 1. While the CG-60 coating covers the expanded mesh in such a way that it can be assumed that the MEA does not contact the stainless steel base, the insets of cross-sections CG-48 and CG-33 show that in some areas, contact between the MEA and stainless steel cannot be ruled out.

The total thickness of the coated PTLs was measured using a thickness gauge (DM2010 from Wolf Messtechnik GmbH, Germany) with a resolution of 1 µm and an accuracy of 4 µm [26]. Table 1 summarizes PTL and coating thicknesses.

As visible from Table 1, the maximum thickness of the coating amounted for approximately twice the layer thickness determined using SEM cross sections. This can be attributed to three effects. On the one hand, the PTLs may bend slightly after the coating process, resulting in the total thickness of the PTL being determined too high with the thickness gauge. Secondly, due to the particle size distribution of the feed powder, the layer does not grow homogeneously, as visible from the cross sections. Furthermore, the gauge measures maxima, whereas the thickness determination using SEM images also includes areas with thinner sections, resulting in a thinner average thickness.

2.4. Magnetron sputtering

All coatings deposited by magnetron sputtering are referred to as "PVD" coatings, as no other physical vapor deposition (PVD) process than sputtering was used. PVD was used to deposit thin Pt-coatings of 37 nm on the surface of titanium CGS-layers and titanium felt benchmark PTLs to avoid titanium oxidation. Additionally, all PTLs were Pt-coated on the FF-facing side, except for CG-48_2, where the coating on the FF-facing side was omitted to investigate whether the corrosion rate increases without coating on the back side of the PTL. Although Pt does not provide long-term corrosion protection for stainless steel [27], the PTLs were coated on the back to minimize effects from the PTL surface facing the flowfield. Pt was deposited with a sputter coater Q150T (Quorum Technologies Ltd, United Kingdom) at 30 mA and 0.7 Pa under Argon. The sputter time was 360 s and the loading 0.060±0.008 $mg_{Pt}cm^{-2}$. The PTLs CG-33, CG-48_1 and CG-48_2, were coated by an external company (Limedion GmbH, Germany)

with 40 nm Pt on the side facing the MEA also using a PVD process. This PVD process differed from the in house coatings by a substrate preheating process to remove surface water and a sputter etching step prior to the coating process. This process was expected to yield Pt coatings with an improved adhesion, but as no measurable differences in stability and performance could be identified, this aspect will not be discussed further within this study.

2.5. Electrochemical test protocol

First, the cell temperature was elevated to 80 °C. Subsequently, the cell voltage was increased to 1.7 V and then kept constant at 1.7 V for 15 h (conditioning phase). Afterwards, three I–V curves were recorded between 1.45 V to 2.0 V followed by nine impedance spectra within the same range. After that, the cells were continuously operated at 2.0 V followed by repeated recordings of I–V curves and impedance spectra. The duration of constant operation at 2.0 V is indicated at the corresponding measurements and graphs. In addition to the I–V curves at the begin and end of the test, three further curves were recorded with CG-48 and CG-33 after 156.5 h where a short interruption occurred. With CG-48, another three I–V curves were recorded after 420 h, as the ion exchanger material was removed afterwards to investigate whether the concentration of possible corrosion products increases. Impedance spectra were recorded at the begin and end of the experiment and with CG-48 additionally after 420 h. I–V curves were recorded in 20 mV to 30 mV-steps from 1.45 V to 1.55 V and in 50 mV-steps from 1.55 V to 2.0 V. Each voltage step was held for 5 min and the curves were then generated from the mean values of the last 10 measuring points of a voltage step. Impedance spectra were recorded potentiostatically with a HCP 1005 potentiostat (BioLogic, France). The frequency range was 100 mHz to 10 kHz and the amplitude 5 mV. High frequency resistances (HFRs) were derived from equivalent circuit fitting (Calc-Modulus with 100 iterations) with the software ZView® (Scribner LLC). Figure S2 shows the used modified Radles equivalent circuit (LR(RQ)(RQ)). HFRs could be determined with a fit error of less than 1%. Further uncertainties in determining the HFR can be introduced by the phase error of the potentiostat. However, it is assumed that these uncertainties affect all measurements equally and thus the comparison of the resistances is valid.

2.6. Scanning electron microscopy (SEM) and energy dispersive X-ray spectroscopy (EDX)

Cross sections and top views of PTLs were taken with an EVO 15 scanning electron microscope (SEM) from Carl Zeiss AG (Germany) at IMD-2 with a backs scattered electron (BSE) detector. MEAs were imaged under a Gemini Ultra Plus SEM (Carl Zeiss AG, Germany) at IET-4 with a working distance of 8.5 mm and an accelerating voltage of 20.000 keV. For the determination of the elemental composition at the surface of samples, energy-dispersive X-ray (EDX) analysis was carried out with an ULTIM MAX detector (Oxford instruments).

2.7. Inductively coupled plasma optical emission spectroscopy (ICP-OES)

For the analysis of the chemical composition of the 316L expanded metal, two aliquots of approximately 50 mg per sample were dissolved with 3 mL HCl, 1 mL HNO_3 and 0.2 mL HF at approximately 80 °C for 2 h. Each digestion was filled to 50 mL with Milli-Q water. Two parallel dilutions of each digestion solution (200-fold and 10-fold) were prepared with 1% HNO_3 and analyzed with an iCAP 7600 ICP-OES device (Thermo Fisher Scientific Inc.). The carbon, nitrogen, and sulfur content was supplementarily determined via a combustion process at Elementaranalytik Elektrowerk Weisweiler GmbH (Germany).

2.8. Interfacial contact resistance (ICR)

The through-plane resistance of the PTLs was determined before and after PEMWE operation using a 4-wire measurement as described previously [20] (schematic setup see Figure S3). The PTL was placed between two gold-coated copper blocks and two carbon PTLs, which served to compensate for unevenness of the sample PTLs, as the carbon paper is compressible. 5.8 bar were applied by means of a pneumatic cylinder. According to the manufacturer, the accuracy of the pressure transmitter is specified as 0.5% of the span (10 bar), corresponding to 0.05 bar. The carbon PTLs were initially precompressed 6 times without the sample PTL and their resistance value was determined as the system resistance. The measurement consisted of recording the voltage drop between the two copper blocks at a current of 100 mA, 200 mA, 300 mA, 400 mA, 500 mA, 600 mA, 700 mA and 790 mA applied for 1 s. The sampling rate of the voltage was 0.2 s. The slope of the I–V curve can be assigned to the contact resistances between the interfaces. Thereby, it is assumed that the bulk resistance is negligible compared to the contact resistances. Multiplication with the geometric area of 17.64 cm^2 results in the interfacial contact resistance (ICR).

3. Results and discussion

This section is structured by first discussing the results with the thickest corrosion protection layer. Subsequently, results from the reduction of the layer thickness are discussed.

3.1. Corrosion stability of 316l expanded metals with 60±12 μm titanium CGS coatings

Although it can be anticipated that the protective layer between the PTL and the anode catalyst layer should be as thick as the zone of anodic polarization (up to 200 μm [28]), it had to be guaranteed that the openings of the expanded metal are not sealed by the coating. Therefore, a mean layer thickness of 60 μm (CG-60) was chosen. With these coatings, the layer was dense enough to prevent contact between the CL and the expanded metal, while the openings of the expanded metal remained sufficiently open for media transport. Photographs of post mortem CG-60 PTLs are given in Figure S8. As the coating also partially covered the inner surfaces of the expanded metal (c.f. Fig. 1), it can be assumed that no contact could be established between the CL and 316L expanded metal, even after swelling of the MEA into the structure of the PTL.

Fig. 2 presents mean I–V curves and the high frequency resistances from two parallel experiments with 60±12 μm coated 316L expanded metal PTLs (CG-60). Both, the I–V curves and the development of the HFRs reflect an increased cell performance after 1006 h at a cell voltage of 2.0 V. Furthermore, the performance at the end of test was close to the performance with a benchmark Pt coated titanium felt PTL (gray curve). The reason for the performance increase might stem from the adaptation of the MEA to the non-uniform structure of the CGS-layer, as during the adaptation of the MEA to the PTL surface, the contact area and thus the amount of active catalyst sites used increased. This adaptation process can take several hundred hours [29]. Similarly, microporous layers (MPLs) are used to reduce ohmic losses [30,31]. In addition to the adaptation of the MEA to the PTL, the thickness of the membrane may be slightly decreased due to local creeping [32]. Furthermore, as the charge transfer resistances (CTR) remained almost unchanged (see Figure S11), it is supported, that the increasing current density was primarily caused by decreasing ohmic losses. Additionally, performance improvement due to increased catalyst activity can be excluded, as the iR-free cell voltage at 2.5 A cm^{-2} only dropped by about 14 mV (Figure S12).

Also with benchmark PTLs a slight improvement in performance could be observed after 457 h at 2.0 V, but significantly less pronounced (Figure S5a [20]). While the increase in current density at 2.0 V was

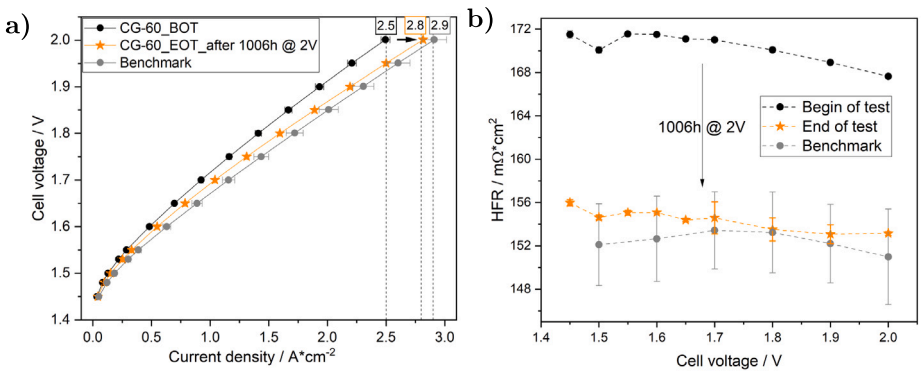

Fig. 2. (a) Mean I–V curves at the begin of test (BOT) and after 1006 h at 2.0 V (EOT) of two PEMWE single cells with 60±12 µm Ti coated 316L expanded metal anode PTLs compared with a reference Pt coated Ti felt PTL (benchmark); (b) Corresponding HFRs in dependence of the cell voltage.

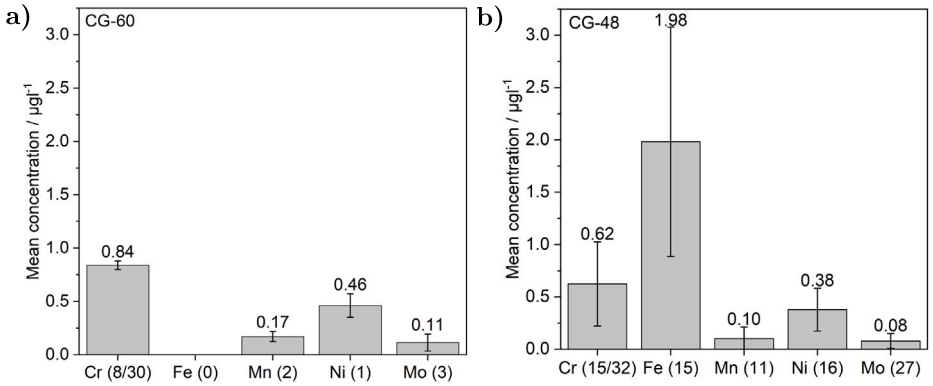

Fig. 3. Mean concentrations of Fe, Cr, Mn, Ni and Mo from the anode and cathode outlet during 1006 h and 1004 h PEMWE single cell tests at 2.0 V with 316L expanded metal anode PTLs with (a) 60±12 µm coated PTLs (CG-60) and (b) 48(16) µm coated PTLs (CG-48). The number of samples in which the respective analyte was found are indicated in brackets.

0.04 A cm^{-2} for the benchmark after 457 h, the increase with the CGS-coated PTLs amounted for 0.4 A cm^{-2} after 1006 h. It was also verified that the CGS coating improved the performance compared to expanded metals coated purely with Pt, as the performance with Pt coated titanium expanded metal PTLs almost did not change during 457 h of operation (Figure S5b). Additionally, performance improvement after 536 h of operation was also visible with a CGS-coated titanium expanded metal, see Figure S6b. Consequently, the performance improvement can be attributed to the properties of the coating. No mass transport limitation was visible from impedance data at the begin and end of the experiment (Figures S9a, S9b, S10a and S10b). In addition, it can be ruled out that membrane thinning led to decreasing HFRs, as the membrane thickness measured post mortem was similar to membranes that were operated with pure titanium PTLs and a similar test duration (see supporting information Table S1).

Furthermore, inductively coupled plasma mass spectrometry (ICP-MS) was used to monitor if any corrosion products like iron, chromium, nickel, manganese or molybdenum ions were released from the PTLs. For this purpose, water samples were taken directly from the anode and cathode outlets of the cells during operation (effluent water) as well as samples from the storage tanks before and after the experiments. Test bench components can be ruled out as a source of Fe, Cr, Ni, Mn, and Mo ions, as no stainless steel components are used. Fig. 3a shows the mean concentrations of the two experiments with CG-60 and Fig. 3b with CG-48_1 and CG-48_2. For this purpose, the concentrations determined from the experiments with CG-48 were combined, as the concentrations were of the same order of magnitude. Individual concentrations of the two experiments with CG-48 can be found in the supplementary information Figure S19. During the experiments with CG-60, no Fe (detection limit 0.3 µg L^{-1}) and only small amounts of Cr in 8 out of 30 samples (0.84±0.04 µg L^{-1}), Mn in 2 out of 30 samples (0.17±0.05 µg L^{-1}) and Ni in one sample (0.46±0.1 µg L^{-1}) were detected in the effluent water (Fig. 3a). Detecting chromium is probable, as it is the most abundant element at the surface of 316L [33]. However, all concentrations stayed below concentrations that were found in Milli-Q water exposed to an uncoated 316L expanded metal for about 90 h at 80 °C and 80 h at room temperature (Figure S7). Furthermore, the storage tanks remained free from corrosion products above the detection limit in the sub-ppb-range, indicating that no severe pitting corrosion of the 316L base took place. As ICP-MS can only detect contaminants that are dissolved, post mortem EDX spectra of MEA cross sections were captured complementary. No stainless steel components were found in more than 400 spectra from MEA cross sections, further supporting the stability of the PTLs. Upon examination of the PTL post mortem, almost no changes could be detected. Only about 0.06% of the surface of the PTL back showed rust-colored changes (Figure S8b). This form of surface corrosion can occur due to exposure to ultra pure water [34] and is promoted by the prevailing oxygen atmosphere. However, as no influence of corrosion products on electrolysis performance or impedance was observed, it can be assumed that the metal ions dissolved from the FF-facing side of the PTL were washed out faster by the flowing water than they could migrate to the CL.

Based on the I–V curves, impedance spectra and EDX analysis of membrane cross-sections, we conclude that, despite occasional low concentrations of Cr, Mn and Ni in the effluent water, titanium can be partially replaced by a stainless steel-based PTL provided a sufficiently thick corrosion protection layer is applied. Our observation that a 60±12 µm CGS-layer can sufficiently protect a stainless steel PTLs against corrosion is consistent with the results from Stiber et al. [12],

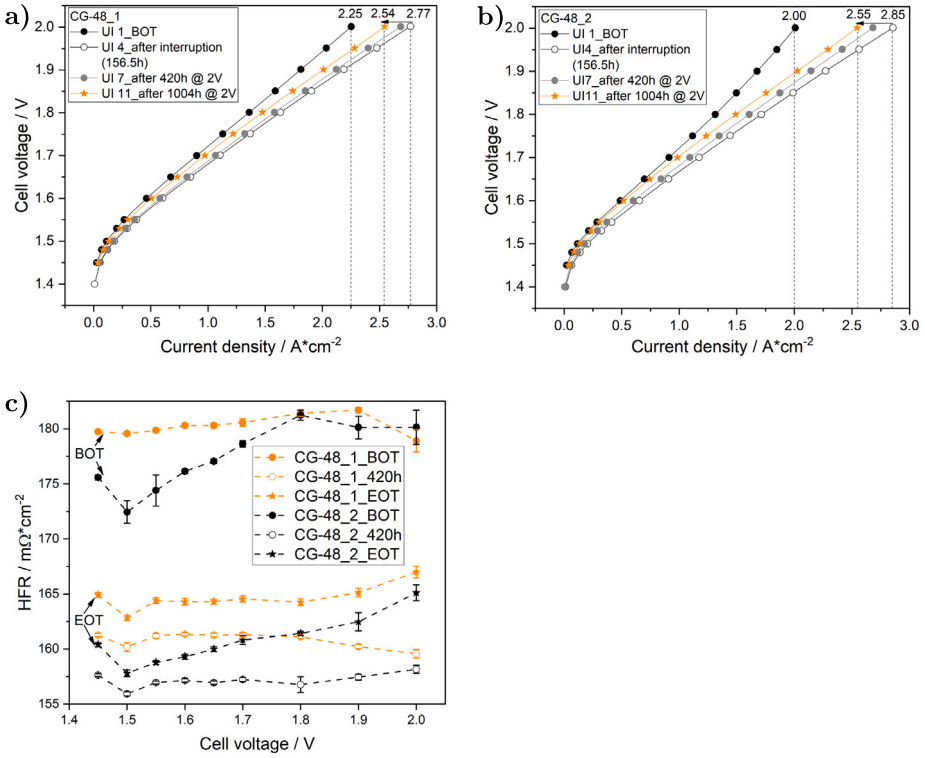

Fig. 4. (a) and (b) I–V curves at the begin of test (BOT), after a short test bench interruption after 156.5 h (UI 4), after 420 h (UI 7) and after 1004 h (UI 11) of two PEMWE single cells operated with 48±16 μm Ti coated 316L expanded metal anode PTLs; (c) HFRs in dependence of the cell voltage for cells with the anode PTLs CG-48_1 and CG-48_2 at the begin of test, after 420 h and 1004 h (EOT).

who also reported no corrosion with vacuum plasma sprayed (VPS) coatings on 316L expanded metals with a cumulative thickness of the Ti and Nb coating of about 24 μm to 94 μm and with Gago et al. [27] who showed that a 60 μm thick Ti coating produced by VPS is sufficient to provide protection for stainless steel bipolar plates in PEM electrolysers.

Furthermore, we calculated that our layered PTLs, consisting of a stainless steel expanded metal and titanium coating, can save around minimum 25% Ti compared to a benchmark full titanium PTL. The saving can even be increased to 58% in case of 100% recovery of the titanium powder that is not deposited on the sample. These calculations are based on the assumption that the density of the titanium felt PTL (360 μm thick), calculated with its average porosity of 68% and weight, is 51.8 $mg_{Ti}cm^{-2}$ and the specific weight of the 60±12 μm CGS-coating amounts for 21.6 $mg_{Ti}cm^{-2}$. The deposition efficiency of the titanium powder was measured to be 80%. As the open area of the expanded metal is 25%, the total deposition efficiency is 55%. Thereby, the titanium savings calculated assume an idealized process. As the aim of the work was to experimentally investigate whether and under what conditions PTLs made of stainless steel with cold-sprayed corrosion protection coatings can be used in PEMWE operation, the indications of possible titanium savings serve only as assessment for the approximate savings potential of titanium.

3.2. Corrosion stability of 316L expanded metals with 48±16 μm and 33±16 μm titanium CGS coatings

As the experiments with 60±12 μm coated stainless steel expanded metals enabled 1006 h stable PEMWE operation at 2.0 V, the thickness of the titanium CGS-layer was reduced to 48±16 μm (CG-48) and 33±16 μm (CG-33) to investigate whether corrosion protection can also be achieved with thinner coatings. With the PTLs CG-48, experiments were conducted for 1004 h at 2.0 V, whereby the ion exchange resins were removed after 420 h to accumulate possible corrosion products in the water tanks.

The experiment with CG-33 was shortened to 362 h, as the corrosion of iron was visible in the form of reddish deposits at the cell outlets. Results with two cells with 48±16 μm coated PTLs (CG-48_1 and CG-48_2) will be discussed first.

Unlike the measurements with CG-60, the two parallel experiments with CG-48 were not combined into mean values, as the current densities differed significantly at the beginning of the experiment for reasons that are unknown. These differences are presumably attributable to different overvoltages for charge transfer (see Figure S14), as the ohmic resistances at the begin of the test in the high current density range above 1.8 V did not show any significant difference (see Fig. 4c). Although an initial increase in performance was also visible with thinner Ti layers, see UI 4 (I–V curve number 4) in Fig. 4a and b, the cell performance dropped until 420 h and furthermore until the end of experiment at 1004 h. The development of the high frequency resistances revealed a similar trend (Fig. 4c). At the BOT, the mean HFRs amounted for 180.3±1 $m\Omega\,cm^2$ (CG-48_1) and 177.3±3 $m\Omega\,cm^2$ (CG-48_2). After 420 h, the cell resistances dropped to 160.8±1 $m\Omega\,cm^2$ and 157±1 $m\Omega\,cm^2$ respectively and slightly increased again to 164.6±1 $m\Omega\,cm^2$ and 160.7±2 $m\Omega\,cm^2$ after 1004 h. At the end of test, the HFRs at 1.9 V and 2.0 V were slightly higher than at lower potentials, indicating the blockage of proton channels that are especially needed at higher current densities. A higher HFR at higher current densities in presence of 5 $\mu g\,L^{-1}$ Ca^{2+} contamination was also reported by Padgett et al. [8]. In general, a decreasing trend of the CT resistance between the spectra at the BOT and after 420 h and an increasing trend between the spectra at 420 h and at the end of the test was observed. Nyquist plots are given in Figure S17 and S18. With CG-48_2, an additional feature at low frequencies was discerned above 1.8 V. In addition, increased low-frequency resistances (LFRs) were observed with CG-48_1 above 1.9 V. This shift of the LFR towards higher resistances can be attributed to an additional feature at low frequencies, pointing to cationic contamination [8]. Furthermore, the iR-free cell voltage decreased slightly after 420 h, indicating a slight

increase in catalyst activity, but increased towards the end of test, thus changed only minimally throughout the experiment (Figure S16). Consequently, the activation overvoltage fluctuated, but with iR-free curves, no permanent catalyst inactivation could be proven.

Compared to the experiments with CG-60, iron was detected in the effluent water (see Fig. 3b), potentially explaining the loss of performance and pointing towards a higher corrosion rate compared to CG-60 PTLs. The concentration of all other 316L components like Cr, Mn, Ni and Mo was in the same range as with CG-60, but were present in more samples, indicating a higher rate of corrosion. Although the cell with the PTL CG-48_2 operated at elevated temperatures between 81 °C to 86 °C over the last 450 h (temperature curve see Figure S13), the concentrations of corrosion products were in a similar range than with the PTL CG-48_1.

As standard, the water is filtered using ion exchangers before it is delivered to the cell. To investigate if any corrosion products accumulate during the experiments with reduced titanium coatings of 33±16 µm and 48±16 µm, the ion exchanger material was removed after 420 h of operation. Removing the ion exchange material resulted in the following effects on cationic impurities: While the concentrations of Na, Mg, K and Al did not increase, the concentration of Ca significantly increased from maximum 12±7 µg L^{-1} to an average of 56±5 µg L^{-1} and maximum of 115±9 µg L^{-1}. Calcium could be accumulated from the glass heat exchanger. Another source of Ca could be the production of the Nafion™ membrane, as Ca^{2+} or Na^{+} are potentially being used to stabilize the dispersion [35]. However, these high concentrations are likely to involve additional sources of calcium. However, it can be assumed that the influence of Ca^{2+} on electrolysis performance is low as the cells were operated at a high current density where Ca^{2+} ions are known to get removed from the cell [8]. In MEA cross sections, Ca was detected up to 1 at.% with one exception of 2.4 at.% at one point in an anode CL, but as no effects on cell performance were observed with other MEAs containing Ca in similar concentrations, it can be assumed that Ca contamination was not the cause for the performance reduction.

Ni and Mn concentrations in the effluent water were not higher within experiments with CG-48 compared to CG-60, but the amount of contaminated samples was significantly higher (elevated twice and 16 times, see Fig. 3). Consequently, it can be assumed, that CG-48 PTLs were affected by corrosion with a higher rate than CG-60. Furthermore, more samples contained Mn (2 vs. 11) and Ni (1 vs. 27) and Fe were found within experiments with CG-48, which was not the case in experiments with CG-60.

In addition, post mortem MEA cross sections revealed that the thickness of the membrane was reduced compared to MEAs operated with CG-60 or pure titanium PTLs (see supporting information Table S1). This is another indicator of corrosion, as iron and chromium ions migrating to the cathode side can catalyze the formation of radicals via Fenton reactions that attack the polymer and hence contribute to membrane thinning [36–38]. A further mechanism of membrane degradation, also catalyzed by iron ions, was described by Tsuneda [39].

Another indicator of PTL degradation is the interfacial contact resistance (ICR) determined before and after the experiments. While the increase of the ICR of CG-60 and CG-48_1 ranged between 1.23 mΩ cm^2 and 1.61 mΩ cm^2, the ICR of CG-48_2 that experienced a higher cell temperature was significantly higher, as the increase amounted for 47 mΩ cm^2 (Fig. 5) and tarnish colors on the back side were visible (Figure S15c). However, the ohmic resistance (HFR) did not increase more with this PTL than with the other PTLs. Consequently, the ICR can give an indication of changes in PTL conductivity, but other factors, which are not part of the ICR measurement setup, such as the contact with the FF can lead to different resistances within the PEMWE cell. Furthermore, more areas of surface corrosion were found on the back of CG-48 PTLs compared to CG-60 PTLs, pointing to a superior stability of the PTLs with thicker protective coatings (see Figures S8 and S15).

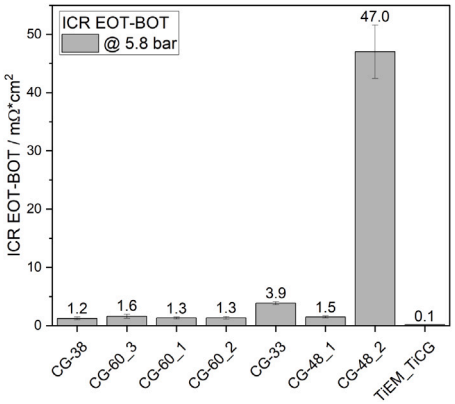

Fig. 5. Increase of the interfacial contact resistance determined at a pressure of 5.8 bar before and after PEMWE experiments with 316L expanded metal PTLs with 38±16 µm (CG-38), 33±16 µm (CG-33), 60±12 µm (CG-60) and 48±16 µm (CG-48) titanium cold gas sprayed coatings. Results from PEMWE experiments with CG-38 were published elsewhere [13]. The resistance with a Ti-CGS-coated titanium expanded metal (TiEM_TiCG) is given for comparison with stainless steel based PTLs.

The initial performance with CG-33 was in the same range as all other Ti coated 316L expanded metal anode PTLs (2.39 A cm^{-2}, Fig. 6a vs. 2.0 A cm^{-2} to 2.5 A cm^{-2}, Fig. 2 and Fig. 4a and b). Furthermore, an initial performance increase was visible (UI 4), but after an interruption (156.5 h at 2.0 V), the pump stopped working and the water supply was interrupted for 62.5 h. After dry running, the water supply was re-established and the cell further operated at 2.0 V, but the cell performance dropped and therefore the experiment was terminated after 362 h total operating hours. In one water sample before the pump failure, high concentrations of iron (170±20 µg L^{-1}), manganese (11.1±0.2 µg L^{-1}) and nickel (12.7±0.3 µg L^{-1}) were detected in the effluent water at the cathode side (see sample C3 Figure S22a) and corrosion of iron became visible in form of reddish deposits at the cathode outlet. Furthermore, Ni accumulated in the storage tank where the concentration increased to 4.31±0.14 µg L^{-1}. SEM cross sections revealed, that the surface of the expanded metal was affected by corrosion beneath the titanium coating (Fig. 6b), which was not observed with CG-48 and CG-60. Consequently, the 33±16 µm coating was not thick or dense enough to protect against corrosion or the combination of an insufficient thickness and coverage (see Fig. 1) resulted in poor corrosion protection. Furthermore, it is conceivable that the MEA swelled deep enough into the openings of the PTL to get into contact with uncoated areas of the expanded metal with the CL inducing corrosion (see Fig. 1.

Further indication of corrosion was visible from impedance data, as cation poisoning of the membrane was evident from Nyquist plots by increased low frequency resistances (Fig. 7a and b). At the begin of test after 15 h conditioning at 1.7 V, the CTR only decreased up to 1.65 V, stayed constant between 1.65 V to 1.8 V and increased above 1.8 V (Fig. 7a). High CTRs were even more visible in the spectra at the end of test (Fig. 7b), where the CTRs only decreased up to 1.6 V and stayed constant up to 2.0 V. As described above, these features at low frequencies are associated with cation poisoning of the membrane leading to proton depletion at the cathode side [8]. CTRs increased not only with increasing current density, but also over time (see Figure S21). Increasing CTRs from the begin to the end of the experiment is a further indication of cation contamination.

4. Conclusions

The corrosion stability of anode PTLs for PEM water electrolysis composed of 316L expanded metals with 33±16 µm (CG-33),

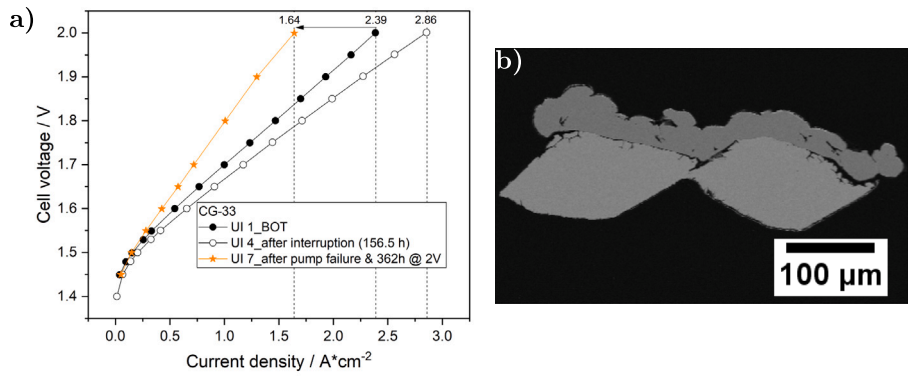

Fig. 6. (a) I–V curves at the begin of test (BOT), after a test bench interruption (156.5 h, UI 4) and after 362 h (UI 7) at 2.0 V of a PEMWE single cell operated with CG-33; (b) post mortem SEM cross section of CG-33. Post mortem cross sections of CG-48 and CG-60 are given in Figure S20 for comparison.

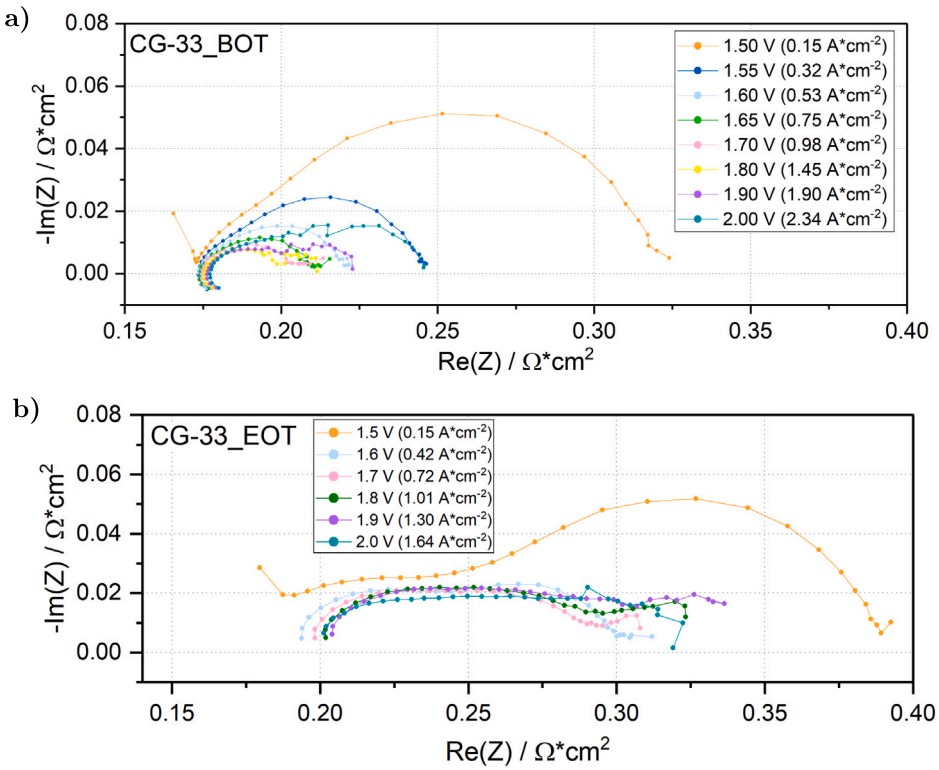

Fig. 7. Impedance spectra of a PEMWE single cell operated with 33±16 µm Ti coated 316L expanded metal anode PTL at the begin of test (BOT); b) at the end of test (EOT) after 362 h at 2.0 V, of which 62.5 h without water supply.

48±16 µm (CG-48) and 60±12 µm (CG-60) titanium cold gas sprayed coatings (CGS) for corrosion protection was investigated. To reduce the contact resistance, a thin platinum layer of 37.5 nm was sputtered on top.

Their corrosion stability was evaluated by PEMWE single cell experiments at a constant cell voltage of 2.0 V for 362 h to 1006 h accompanied by impedance spectroscopy and ex situ analytics of water samples as well as post mortem analysis of the MEAs. With CG-60, the cell performance increased to 2.8 A cm^{-2} at 2.0 V during operation for 1006 h and was thus in the same range as Pt-coated benchmark titanium PTLs (2.9 A cm^{-2}). The increased performance compared to expanded metal PTLs without CGS coating is attributable to the CGS coating as it increases the contact area between the PTL and CL. With CG-48, an initial performance increase to 2.8 A cm^{-2} was also observed, but the current density dropped to 2.55 A cm^{-2} by the end of the experiment (1004 h). An even more pronounced drop was observed with CG-33. These trends can be explained by an increasing degree of corrosion, when reducing the thickness of the corrosion protection coating.

While the Ti-coated sides of the PTLs facing the catalyst layer appeared unchanged after the experiments, visible surface corrosion occurred on the sides facing the FF, where only a thin Pt coating was present. This superficial corrosion was most likely caused by contact with oxygen-saturated ultrapure water and can potentially occur on all surfaces of the expanded metal that are not coated with a protective Ti-coating. On the FF-facing sides of CG-60 PTLs, only few small discolored areas were visible (< 1% of the total area facing the FF) and no influences of corrosion products on I–V curves and impedance were observed during the experiments. Consequently, it can be assumed that within these experiments occasional emitted metal cations were removed by the water flow faster than they could migrate to the catalyst layer and thus did not influence cell performance in any quantifiable way.

On the FF-facing side of CG-48 surface corrosion was more pronounced, additionally indicating that a thicker coating of average 60 μm is necessary for sufficient corrosion protection of the stainless steel base. Furthermore, no iron was found in the effluent water from experiments with CG-60. In contrast, half of all water samples from the experiments with CG-48 PTLs contained Cr, Fe and Ni. These contaminations were found in samples from the cathode outlet, proving the migration of cations from the anode to the cathode side. The increased number of contaminated samples and the release of Fe during the experiments with CG-48 confirmed an increased corrosion rate compared to the experiments with CG-60 PTLs. EDX analysis of MEA cross sections further supported this trend as MEAs operated with CG-48 contained iron in the anode catalyst layer while MEAs operated with CG-60 PTLs remained free from stainless steel components. At the cathode side, iron can catalyze the decomposition of the membrane leading to membrane thinning. Membrane thinning was observed with MEAs operated with CG-48, as these membranes exhibited on average a 18% decreased thickness compared to MEAs that were operated with CG-60 and pure titanium PTLs (on average 180 μm vs. on average 220 μm). However, the highest observed degree of corrosion can be attributed to CG-33, as SEM cross sections of CG-33 revealed corrosion clearly visible beneath the titanium coating.

As a result, 316L based PTLs might be only an alternative to full body titanium PTLs when a sufficient thick corrosion protection layer of average 60 μm is applied. With cold gas spraying, we chose a cost-effective coating technique and with CG-60 PTLs up to 58% titanium can be saved in case of 100% recovery of titanium powder compared to benchmark titanium felt PTLs.

With our work, we started a holistic consideration of 316L based PTLs, including a detailed analysis of corrosion products in the effluent water and in MEAs and their influence on cell performance development and impedance, setting a starting point for further critical discussion on the use of stainless steel as a base material for anode PTLs.

5. Outlook

As the current density with the membrane used (Nafion™ 117) is limited to 2.9 A cm^{-2}, research beyond this study should investigate if with thinner membranes and higher current densities where locally higher temperatures occur the corrosion stability of stainless steel based PTLs can further be guaranteed. Additionally, further experiments with PEMWE stacks are necessary. Only if these tests confirm that no detrimental amounts of corrosion products are emitted by contact with ultrapure water, stainless steel will be suitable as a base for anode PTLs in PEM water electrolysis. To scale-up, the CGS coatings need to be further developed towards a more homogeneous thickness over the entire coating area. This can be achieved with a titanium powder with a smaller particle size and a narrower particle size distribution, whereby costs and benefits must be weighed up. In addition, for scaling to expanded metals with larger size, it must be ensured that no bending of the expanded metal takes place and that no deformations occur during the deposition process that would be detrimental to zero-gap PEMWE cell stacking.

CRediT authorship contribution statement

Sarah Zerressen: Writing – review & editing, Writing – original draft, Visualization, Validation, Methodology, Investigation, Formal analysis, Data curation, Conceptualization. **Tim Sievert:** Writing – review & editing, Visualization, Resources, Methodology, Investigation. **Andreas Glüsen:** Writing – review & editing, Supervision, Resources, Project administration, Funding acquisition, Conceptualization. **Martin Müller:** Funding acquisition, Conceptualization. **Robert Vaßen:** Writing – review & editing, Supervision, Resources, Project administration, Funding acquisition. **Ralf Peters:** Writing – review & editing, Supervision. **Ulf-Peter Apfel:** Writing – review & editing, Supervision.

Declaration of competing interest

The authors declare that they have no known competing financial interests or personal relationships that could have appeared to influence the work reported in this paper.

Acknowledgments

We acknowledge financial support by the German Federal Ministry of Research, Technology and Space (BMFTR) in the framework of the project "Wasserstoff: Elektrolyse – Elektrochemische Wasserstofferzeugung der nächsten Generation (HyInnoLyze)", grant agreement 03ZU1115AA and within the project "HylnnoCells — WASSERSTOFF: Flexible Produktion elektrochemischer Zellen — C", grant agreement 03ZU1115JC.

Open access funding is provided by the Deutsche Forschungsgemeinschaft (DFG, German Research Foundation), Germany – 491111 487. Furthermore, we gratefully acknowledge the preparation of membrane electrode assemblies by Daniel Holtz (Forschungszentrum Jülich GmbH, IET-4), Andreas Everwand for acquiring SEM images and EDX spectra (Forschungszentrum Jülich GmbH, IET-4), Florian Seidler for taking post mortem photographs of the PTLs (Forschungszentrum Jülich GmbH, IET-4), Nadine Wettengl (Forschungszentrum Jülich GmbH, IMD-2) and Sabine Willbold (Forschungszentrum Jülich GmbH, IBI-7) for ICP-OES measurements as well as the production of the expanded metal used by Klaus Bender (Bender GmbH Maschinenbau u. Streckmetallfabrik, Siegen, Germany).

Appendix A. Supplementary data

Supplementary material related to this article can be found online at https://doi.org/10.1016/j.jpowsour.2026.239846.

Data availability

Data will be made available on request.

References

[1] A.M. Oliveira, R.R. Beswick, Y. Yan, A green hydrogen economy for a renewable energy society, Curr. Opin. Chem. Eng. 33 (2021) 100701, http://dx.doi.org/10.1016/j.coche.2021.100701.

[2] G. Franchi, M. Capocelli, M. de Falco, V. Piemonte, D. Barba, Hydrogen production via steam reforming: A critical analysis of MR and RMM technologies, Membranes 10 (1) (2020) 10, http://dx.doi.org/10.3390/membranes10010010.

[3] H. Sayed-Ahmed, Á. Toldy, A. Santasalo-Aarnio, Dynamic operation of proton exchange membrane electrolyzers—Critical review, Renew. Sustain. Energy Rev. 189 (2024) 113883, http://dx.doi.org/10.1016/j.rser.2023.113883.

[4] A. Badgett, M. Ruth, B. James, B. Pivovar, Methods identifying cost reduction potential for water electrolysis systems, Curr. Opin. Chem. Eng. 33 (2021) 100714, http://dx.doi.org/10.1016/j.coche.2021.100714.

[5] M. Langemann, D.L. Fritz, M. Müller, D. Stolten, Validation and characterization of suitable materials for bipolar plates in PEM water electrolysis, vol. 40, 2015, http://dx.doi.org/10.1016/j.ijhydene.2015.04.155.

[6] M. Langemann, Bipolarplattenmaterialien für Polymer-Elektrolyt-Membran Elektrolyse (Ph.D. thesis), RWTH Aachen University, Aachen, ISBN: 978-3-95806-192-7, 2016.

[7] N. Rojas, M. Sánchez-Molina, G. Sevilla, E. Amores, E. Almandoz, J. Esparza, M.R. Cruz Vivas, C. Colominas, Coated stainless steels evaluation for bipolar plates in PEM water electrolysis conditions, Int. J. Hydrog. Energy 46 (51) (2021) 25929–25943, http://dx.doi.org/10.1016/j.ijhydene.2021.03.100.

[8] E. Padgett, A. Adesso, H. Yu, J. Wrubel, G. Bender, B. Pivovar, S.M. Alia, Performance losses and current-driven recovery from cation contaminants in PEM water electrolysis, J. Electrochem. Soc. 171 (6) (2024) 064510, http://dx.doi.org/10.1149/1945-7111/ad576b.

[9] P. Lettenmeier, R. Wang, R. Abouatallah, F. Burggraf, A.S. Gago, K.A. Friedrich, Coated stainless steel bipolar plates for proton exchange membrane electrolyzers, J. Electrochem. Soc. 163 (11) (2016) F3119–F3124, http://dx.doi.org/10.1149/2.0141611jes.

[10] J. Mo, S.M. Steen, F.-Y. Zhang, T.J. Toops, M.P. Brady, J.B. Green, Electrochemical investigation of stainless steel corrosion in a proton exchange membrane electrolyzer cell, Int. J. Hydrog. Energy 40 (36) (2015) 12506–12511, http://dx.doi.org/10.1016/j.ijhydene.2015.07.061.

[11] N.F. Daudt, F.J. Hackemüller, M. Bram, Powder metallurgical production of 316l stainless steel/niobium composites for proton exchange membrane electrolysis cells, Powder Metall. 62 (3) (2019) 176–185, http://dx.doi.org/10.1080/00325899.2019.1607461.

[12] S. Stiber, N. Sata, T. Morawietz, S.A. Ansar, T. Jahnke, J.K. Lee, A. Bazylak, A. Fallisch, A.S. Gago, K.A. Friedrich, A high-performance, durable and low-cost proton exchange membrane electrolyser with stainless steel components, Energy Environ. Sci. (2022) http://dx.doi.org/10.1039/D1EE02112E.

[13] T. Sievert, S. Zerressen, M. Bram, A. Glüsen, K. Bender, O. Guillon, R. Vaßen, Cold gas spraying of titanium on stainless steel to enhance corrosion protection inside proton exchange membrane water electrolyzers, Surf. Coat. Technol. 513 (2025) 132486, http://dx.doi.org/10.1016/j.surfcoat.2025.132486.

[14] O. Sorsa, J. Nieminen, P. Kauranen, T. Kallio, Stable reference electrode in polymer electrolyte membrane electrolyser for three-electrode measurements, J. Electrochem. Soc. 166 (16) (2019) F1326–F1336, http://dx.doi.org/10.1149/2.0461916jes.

[15] L.V. Bühre, S. Bullerdiek, P. Trinke, B. Bensmann, A.-L.E.R. Deutsch, P. Behrens, R. Hanke-Rauschenbach, Application and analysis of a salt bridge reference electrode setup for PEM water electrolysis: Towards an extended voltage loss break down, J. Electrochem. Soc. 169 (12) (2022) 124513, http://dx.doi.org/10.1149/1945-7111/ac9ee1.

[16] E. Wallnöfer-Ogris, I. Grimmer, M. Ranz, M. Höglinger, S. Kartusch, J. Rauh, M.-G. Macherhammer, B. Grabner, A. Trattner, A review on understanding and identifying degradation mechanisms in PEM water electrolysis cells: Insights for stack application, development, and research, Int. J. Hydrog. Energy 65 (2024) 381–397, http://dx.doi.org/10.1016/j.ijhydene.2024.04.017.

[17] M. Bram, A. Glüsen, Final report on the project "Neuartige kostengünstige Stromkollektoren für die PEM-Elektrolyse zur Herstellung von Wasserstoff aus regenerativen Energien" (NeStPEL II), 2021, http://dx.doi.org/10.2314/KXP:1837867755.

[18] C.G. Rakousky, Langzeitstabilität der Polymerelektrolyt-Wasserelektrolyse bei reduziertem Iridiumgehalt (Ph.D. thesis), RWTH Aachen University, Aachen, 2016.

[19] S.-V. Pape, S. Zerressen, M.F. Seidler, R. Keller, F. Lohmann-Richters, M. Müller, U.-P. Apfel, A.K. Mechler, A. Glüsen, Performance data extraction from dynamic long-term operation of proton exchange membrane and alkaline water electrolysis cells, Int. J. Hydrog. Energy 127 (2025) 51–63, http://dx.doi.org/10.1016/j.ijhydene.2025.03.387.

[20] T. Sievert, S. Zerressen, A. Glüsen, M. Bram, S. Uhlenbruck, K. Bender, F. Vondahlen, P. Xiao, X. Cao, O. Guillon, R. Peters, M. Müller, U.-P. Apfel, R. Vaßen, TiNb alloy coatings for anode PTLs in PEM water electrolyzers, J. Power Sources 664 (2026) 238944, http://dx.doi.org/10.1016/j.jpowsour.2025.238944.

[21] T. Hussain, Cold spraying of titanium: A review of bonding mechanisms, microstructure and properties, Key Eng. Mater. 533 (2012) 53–90, http://dx.doi.org/10.4028/www.scientific.net/KEM.533.53.

[22] W. Żórawski, R. Molak, J. Mądry, J. Sienicki, A. Góral, M. Makrenek, M. Scendo, R. Dobosz, Experimental and numerical investigations of titanium deposition for cold spray additive manufacturing as a function of standoff distance, Materials 14 (19) (2021) 5492, http://dx.doi.org/10.3390/ma14195492.

[23] C. Liu, Noble Metal Coated Porous Transport Layers for Polymer Electrolyte Membrane Water Electrolysis (Ph.D. thesis), RWTH Aachen University, Aachen, ISBN: 978-3-95806-603-8, 2021.

[24] T. Bautkinova, N. Utsch, T. Bystron, M. Lhotka, M. Kohoutkova, M. Shviro, K. Bouzek, Introducing titanium hydride on porous transport layer for more energy efficient water electrolysis with proton exchange membrane, J. Power Sources 565 (2023) 232913, http://dx.doi.org/10.1016/j.jpowsour.2023.232913.

[25] T. Sievert, Entwicklung von Korrosionsschutzschichten für PEM-Elektrolyseure: Publication in progress (Ph.D. thesis), Ruhr-Universität Bochum, Bochum, 2025.

[26] M. Stähler, I. Friedrich, Statistical investigations of basis weight and thickness distribution of continuously produced fuel cell electrodes, J. Power Sources 242 (2013) 425–437, http://dx.doi.org/10.1016/j.jpowsour.2013.05.073.

[27] A.S. Gago, S.A. Ansar, B. Saruhan, U. Schulz, P. Lettenmeier, N.A. Cañas, P. Gazdzicki, T. Morawietz, R. Hiesgen, J. Arnold, K.A. Friedrich, Protective coatings on stainless steel bipolar plates for proton exchange membrane (PEM) electrolysers, J. Power Sources 307 (2016) 815–825, http://dx.doi.org/10.1016/j.jpowsour.2015.12.071.

[28] H. Becker, E.J.F. Dickinson, X. Lu, U. Bexell, S. Proch, C. Moffatt, M. Stenström, G. Smith, G. Hinds, Assessing potential profiles in water electrolysers to minimise titanium use, Energy Environ. Sci. 15 (6) (2022) 2508–2518, http://dx.doi.org/10.1039/D2EE00876A.

[29] C. Rakousky, U. Reimer, K. Wippermann, S. Kuhri, M. Carmo, W. Lueke, D. Stolten, Polymer electrolyte membrane water electrolysis: Restraining degradation in the presence of fluctuating power, J. Power Sources 342 (2017) 38–47, http://dx.doi.org/10.1016/j.jpowsour.2016.11.118.

[30] Z. Kang, G. Yang, J. Mo, S. Yu, D.A. Cullen, S.T. Retterer, T.J. Toops, M.P. Brady, G. Bender, B.S. Pivovar, J.B. Green, F.-Y. Zhang, Developing titanium micro/nano porous layers on planar thin/tunable LGDLs for high-efficiency hydrogen production, Int. J. Hydrog. Energy 43 (31) (2018) 14618–14628, http://dx.doi.org/10.1016/j.ijhydene.2018.05.139.

[31] Z. Kang, S. Yu, G. Yang, Y. Li, G. Bender, B.S. Pivovar, J.B. Green, F.-Y. Zhang, Performance improvement of proton exchange membrane electrolyzer cells by introducing in-plane transport enhancement layers, Electrochim. Acta 316 (2019) 43–51, http://dx.doi.org/10.1016/j.electacta.2019.05.096.

[32] A. Hintzen, M. Stähler, I. Friedrich, Membrane creep caused by porous transport layer compression in pem water electrolysis and the impact on hydrogen permeation, J. Electrochem. Soc. 172 (4) (2025) 044512, http://dx.doi.org/10.1149/1945-7111/adcd00.

[33] W. Fredriksson, S. Malmgren, T. Gustafsson, M. Gorgoi, K. Edström, Full depth profile of passive films on 316l stainless steel based on high resolution HAXPES in combination with ARXPS, Appl. Surf. Sci. 258 (15) (2012) 5790–5797, http://dx.doi.org/10.1016/j.apsusc.2012.02.099.

[34] A. Mattei, C. Chiavari, E. Bernardi, C. Martini, N. Gandolfi, S. Sessa, M. Bignozzi, Stainless steel corrosion in ultrahigh-purity water: Surface analyses and metal release, in: Proceedings of Eurocorr 2013 (EFC Event N.343), GBR and London and European Federation of Corrosion (EFC), 2013, pp. 1–9.

[35] E.Y. Safronova, D.Y. Voropaeva, D.V. Safronov, N. Stretton, A.V. Parshina, A.B. Yaroslavtsev, Correlation between nafion morphology in various dispersion liquids and properties of the cast membranes, Membranes 13 (1) (2022) 13, http://dx.doi.org/10.3390/membranes13010013.

[36] A. Laconti, H. Liu, C. Mittelsteadt, R. McDonald, Polymer electrolyte membrane degradation mechanisms in fuel cells - findings over the past 30 years and comparison with electrolyzers, ECS Trans. 1 (8) (2006) 199–219, http://dx.doi.org/10.1149/1.2214554.

[37] S.H. Frensch, G. Serre, F. Fouda-Onana, H.C. Jensen, M.L. Christensen, S.S. Araya, S.K. Kæ r, Impact of iron and hydrogen peroxide on membrane degradation for polymer electrolyte membrane water electrolysis: Computational and experimental investigation on fluoride emission, J. Power Sources 420 (2019) 54–62, http://dx.doi.org/10.1016/j.jpowsour.2019.02.076.

[38] T. Kinumoto, M. Inaba, Y. Nakayama, K. Ogata, R. Umebayashi, A. Tasaka, Y. Iriyama, T. Abe, Z. Ogumi, Durability of perfluorinated ionomer membrane against hydrogen peroxide, J. Power Sources 158 (2) (2006) 1222–1228, http://dx.doi.org/10.1016/j.jpowsour.2005.10.043.

[39] T. Tsuneda, Fenton reaction mechanism generating no OH radicals in nafion membrane decomposition, Sci. Rep. 10 (1) (2020) 18144, http://dx.doi.org/10.1038/s41598-020-74646-0.